Photonic Crystal Fiber Sensors, Literature Review, Challenges, and Some Novel Trends

Naira M. Saad, El- Sayed M. El- Rabaie, Ashraf A. M. Khalaf

***Abstract*— This paper introduces an introduction to photonic crystals (PCs) and photonic crystal fiber (PCF) sensors along with their different applications. A comparative study of different types of PCF sensors including chemical, biomedical, and liquid sensors is presented. Many distinct factors, including the device structure, background material, operating wavelength, PCF's guiding mechanisms and the sample refractive indices to be detected, affect how PCF sensors behave. Different topologies such as hexagonal, hollow rectangle, decagonal, rectangular porous core, and mono rectangular are discussed. Sensing properties, and measurement methodologies for each of these sensors are discussed. Based on this comparative study, PCF sensors are categorized according to their properties, topologies, measurement techniques, and applications. The appropriate topology for the required application can be selected based on the required properties. The same PCF topology can be used for different sensing purposes. A comparative study of different types of PCF sensors in a form of table is presented followed by the challenges and some novel trends on Photonic Crystal Fiber.**

***Keywords*— Keywords— PCF Sensors, PCF Types, PCF applications, Hollow-core PCF, Photonic Band Gap PBG effect, Finite Element Method FEM.**

Manuscript received [31Mar. 2023] ; revised [05 May 2023] ; accepted [30 May 2023]. Date of publication [1 July 2023].

Naira M. Saad is with the Department of Management Information Systems Higher Institute of Administrative Sciences Osim, El Giza, Egypt (e-mail: engnaira@yahoo.com).
El- Sayed M. El- Rabaie is with the Department of Electronics and Communications Engineering, Faculty of Electronic Engineering, Menoufia University, Menouf, Egypt P.O. 32952, (e-mail: elsayedelrabaie@gmail.com).
Ashraf A. M. Khalaf is with the Department of Communications and Electronics, Faculty of Engineering, Minia University, Minia, Egypt, P.O. 61111(e-mail: ashkhalaf@yahoo.com)

I. INTRODUCTION

Photonic crystals, a novel class of optical media, represented by artificial structures or natural based on the periodic modulation of the refractive index [1]. Photonic crystals PCs are classified into three basic categories according to their geometrical structure. The first one is the one-dimensional (1D) category which includes the Bragg grating and the anti-reflection optical coatings. The second one is the two-dimensional (2D) which includes waveguides, photonic crystal lasers, photonic crystal fiber, and add/drop filters. Finally, the three-dimensional (3D) such as Opal stone [2]. Fig.1 depicts these three classifications.

Photonic crystal fibers (PCFs) are two-dimensional photonic crystals having a lattice constant with an optical wavelength order. PCFs are a type of microstructure fibers (MFs) or holey fibers. The main distinction between PCFs and those other MFs is that there is a defect in the PCFs core breaks the cladding structure's arrangement on a regular basis. Consequently, PCFs the transmission characteristics are affected by the different refractive indices of defective materials [3].

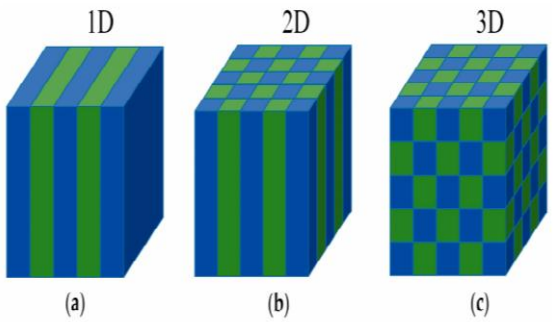

Fig.1. Structures of photonic crystal categories: (a) PCs (1D), (b) PCs (2D) and (c) PCs (3D) [2].

The most significant feature of photonic crystal fibers is that they combine the properties of both 2-D photonic crystals and also conventional fibers. The fiber's features can be largely decided using air hole shape, lattice pitch, the background material refractive index, diameter, and the lattice type.

PCF's two guiding mechanisms are the Index guiding mechanism or total internal reflection TIR-PCFs and the photonic band gap mechanism PBG-PCFs. In the first mechanism, the total internal reflection in the PCFs is nearly equivalent to that found in standard optical fibers. The principle of optical transmission in PBG-PCFs is influenced by the PBG effect which differs from that in both the standard optical fiber and TIR. The cladding structural effects the photons in a specific frequency range due to the band gap, so the beam is able to be transmitted only inside the core [4]. Most of the light beam is bound with a major air hole with a minimum refractive index to achieve low confinement loss [5].

Power fraction, birefringence, and confinement loss are examples of physical properties which can be measured using the PCFs. Waveguide dispersion can be designed and constructed to have zero-dispersion wavelength at any required wavelength, which is beneficial for nonlinear applications. Normal dispersion is a restriction and adjusting the core diameter of the fiber shifts the zero dispersion wavelength in the visible range. For sensing purposes, the PCF can be used for sensing gases or liquids.

Because of their flexible design, PBG hollow-core structures are particularly well suited for sensing applications [6-7]. Furthermore, PCF is now distinguished as a tremendous research trade in sensing applications. Background materials such as TOPAS, TEFON, SILICA, and ZEONOX have been successfully used in photonic crystal fiber to achieve minimal confinement loss and increasing relative sensitivity. Other characteristics that can be obtained include effective mode indexes, effective area, and total power fraction [8]. Because of their ability and superiority, many PCFs have been widely used in chemical, liquid, gas, and biomedical sensing applications in the recent years.

Many essential sectors, such as bio-informatics [9-10], chemical sensor [9-10], bio-Photonics [11-12], medical diagnostics [13-14], temperature sensor [15-16], and other communication areas [17], are now using terahertz (THz) radiation successfully. Terahertz is an electromagnetic spectrum frequency band that includes microwave and infrared radiation ranges from 0.1 to 10 THz.

Recently, the focus has been directed to the photonic crystal fiber porous-core (PCF) [18], which simply allows the calibration of various waveguide factors include the pitch, operating frequency, air-hole radius, and core diameter. Furthermore, by adjusting the waveguide parameters numerically, standard values for optical variables are including dispersion, power fraction PF, effective material loss EML, and confinement loss CL can be obtained; additionally, birefringence can be realized [19].

In this research, the most recent PCF sensor topologies were presented and a comparison was made between various topologies for certain types of PCF sensors.

The remaining parts of the paper are organized as follows: Section II, introduces the different photonic crystal fiber sensor topologies. Section III illustrates the evaluation metrics for PCF sensors. Section IV covers the fabrication feasibilities. Section V shows the numerical mechanisms and commercial software packages available for the simulation of photonic crystal fiber sensors. Section VI summarizes the challenges and some novel trends of PCF followed by the conclusions and the most relevant references.

II. PHOTONIC CRYSTAL FIBER SENSORS TOPOLOGIES

This section gives a review of different photonic crystal fiber (PCF) sensor topologies. PCF sensors topologies are classified as follows:

II.1- Optical Sensor based Photonic Crystal Fiber with Hexagonal Cladding (H-PCF)

H-PCF sensor represents an investigation of a hexagonal cladding with a rotated-hexa core. It is based on an optical sensor structure for chemical sensing with low confinement loss and high sensitivity for chemical sensing features. The designed structure is numerically evaluated using perfectly matched layers (PML) boundary condition and the finite element method (FEM). This mainly aims at improving the optical factors such as effective mode index, effective area, total power fraction, confinement loss, and relative sensitivity over a range of terahertz frequencies (0.80 to 3.0) THz. This H-PCF structure has a lower confinement loss and a higher relative sensitivity contrasted with the earlier PCF [20-21].

At 1 THz, these H-PCF sensor relative sensitivities are 79.22 %, 81.46%, and 82.26%, which are a high relative sensitivities for Water (n = 1.330), Ethanol

(n = 1.354), and Benzene (n = 1.366) respectively. It can also achieve minimal confinement loss of 5.84 $\times 10^{-8}$, 5.85×10^{-8}, and 6.07×10^{-8} dB/m for the same three analytes respectively. Furthermore, the H-PCF structure gains high relative sensitivity and low confinement loss for chemical sensing in bio-medical and industrial applications. Figure 2 depicts the Cross-sectional H-PCF construction [22].

The structure is made up of two layers with circle air holes in a hexa core and five layers of hexagonal cladding with circle air holes. The first layer in the core has six air holes with angles at 20°, 80°, 140°, 200°, 260°, and 320° .The core second layer has 12 circle air holes with angles at 20°, 50°, 80°, 110°, 140°, 170°, 200°, 230°, 260°, 290°, 320°, and 350°. The pitch and the diameter are specified as Λ_c and d_c.

Three different chemicals are used to fill the core. The first is water with n = 1.330, the second is the ethanol with n = 1.354, and the third one is the benzene with n = 1.366. In the cladding, pitch and diameter are represented as Λ_1 and d_1.TOPAS is used as the background material. The percentage of air filled in the cladding region is expressed as d_1/Λ_1. This ratio has the potential to protect the space among the two neighbouring air holes in the cladding. To reduce design implementation complexity, In place of elliptical air holes, circle air holes have been established, particularly in the core.

The parameters of the core two layers are set to get the optimum design. The diameter (d_c) is set to 79 µm, and pitch (Λ_c) is set to 82 µm. The cladding pitch of the five layers is chosen as follows: $\Lambda_1 = 325$ µm and $\Lambda_2 = \Lambda_3 = \Lambda_4 = \Lambda_5 = 350$ µm. The PML thickness is set to 10% of the fiber diameter in order to take control the light reaching the core and going in the direction of the cladding, while avoidance of reflection of the light back into the core.

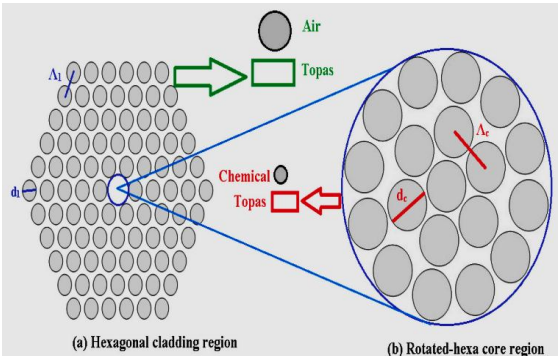

Fig. 2. The H-PCF fiber cross sectional structure: (a) Hexagonal cladding shape and (b) Rotated-hexa core shape [22].

The simulation results are carried out using the methodology in Ref [22] to properly evaluate the effectiveness of the H-PCF. The results are obtained at 1 TH, and it is illustrated that the H-PCF achieves maximum relative sensitivity of 79.22%, 82.26%, and 81.46%, and minimal confinement losses of 5.84×10^{-8}, $6.07\times 10^{-8,}$ and 5.85×10^{-8} dB/m for the three analytes, water, benzene, and ethanol respectively. As a result, it is concluded that the H-PCF sensors can be used primarily for chemical identification in various biomedical applications.

II.2- PCFs with Hollow-Core and Band Gap Cladding

Photonic crystal fibers with hollow-core (HC-PCFs) are used in a variety of applications, which include optical fiber sensing, active optical devices, and communications, due to their excellent optical properties and flexible structure. The structure's arrangement is analyzed using finite elements for the band gap cladding of HC-PCFs and its features [23].

In the C-band, the properties of HC19-1550 and HC-1550-02 are simulated and the HC-1550-02 structural optimization is investigated. Variations in the properties of the optimized HC-1550-02 are investigated over a wavelength range of 1250-1850 nm. The core quartz-ring relative thickness is set to 2.0 and the core radius is adjusted to be 1.8 times the distance between neighboring air holes. Eight cladding layers are used. The sensor achieved very low confinement loss and an extremely high relative sensitivity. This makes it the ideal choice for high sensitivity liquid or gas sensing.

To model and evaluate the properties of the HC19-1550, and HC-1550-02 [24], COMSOL Multiphysics is used as a simulation software, at a wavelength of 1525-1565 nm near C- band, the tube bundle stacking method is used to create HC19-1550 after extracting 19 central capillaries. The focal hole radius is 9.25 µm, the spacing between neighboring air holes (pitch) is set to 3.8 µm, the cladding air hole diameter is set to 3.5 µm, the dimensions of the optical fiber sensing area are set to 73.8 µm, and the PML layer thickness is chosen to be five times the wavelength.

The tube bundle stacking method was used to create the HC-1550-02, and seven central capillaries were extracted and drawn. The parameters of the HC-1550-02 are: The center hole diameter d_c is set to 9.5 µm, the spacing between neighboring air holes Λ_c is set to 3.8 µm,

the cladding air hole diameter d_l is set to 3.5 µm, The diameter of the optical fiber sensing area is set to 70.8 µm, and the PML thickness is set to six times the wavelength λ. Furthermore, RI of PML or the cladding is set to n_{PML} =1.45, nr is the RI of the air hole which is set to 1, and λ/n_{PML} is the standard wavelength for PML. Because of HC-PBG PCF's effect, n_{eff} is set slightly smaller than n_r.

The cross-sectional structure and simulation modelling schematics of HC19-1550 and HC-1550-02 are shown in Fig.3 and Fig.4. The end-face schematics for mode fields of the HC19-1550 and HC-1550-02, as well as the constructed diagrams of both core sections of HC-PCF, are shown in Fig.3, Fig.4 The figure's red arrows clearly shows the electric field direction on the fundamental mode's surface [23].

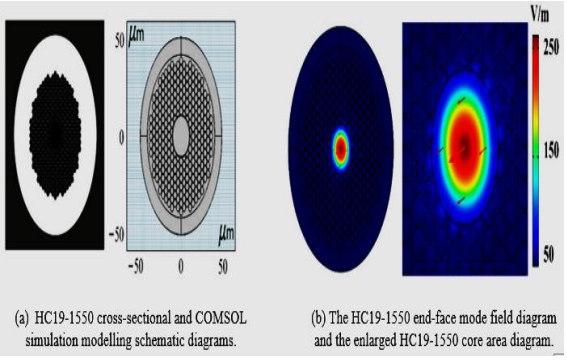

Fig.3. Results of finite element modelling and simulation for HC19-1550 [23].

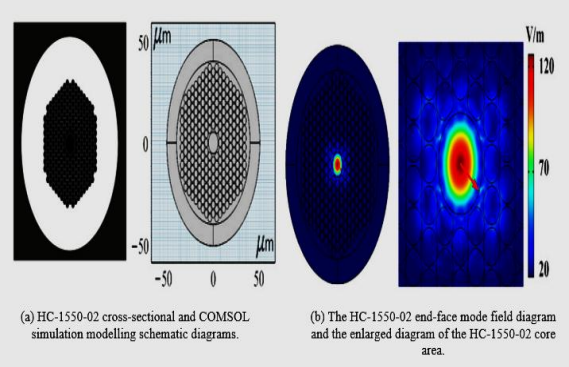

Fig.4. Results of finite element modelling and simulation for HC-1550-02 [23].

The main modes' HC19-1550 and HC-1550-02 mode field areas are 123.05 μm^2 and 36.06 μm^2, respectively, and their core optical power fraction PF are 99.51% and 92.83%, respectively. The HC-PCF air hole area holds the majority of the photon energy, and it has a high concentration primarily in the focal air hole, for just a small amount of the photon energy is bonded to the quartz surface layer in the cladding. As a result, PBG-PCFs are preferred to be used for high-sensitivity sensing. When the two HC-PCF features are compared with wavelength variation in the C-band, it is clear that HC19-1550 has a larger effective mode field area A_{eff}, a lower CL, a higher core optical power, and a higher effective refractive index than HC-1550-02. Its behavior is also more stable.

Fig.5 depicts the main structural design illustration of this structure of band gap cladding HC-PCF with Λ=3.8 µm, d=3.5 µm, R =5 µm, t =0.45 µm, and T =1.5, where R is the radius measured from the core to the inside quartz-ring wall. The value of R is unaffected by varying the core quartz-ring thickness.

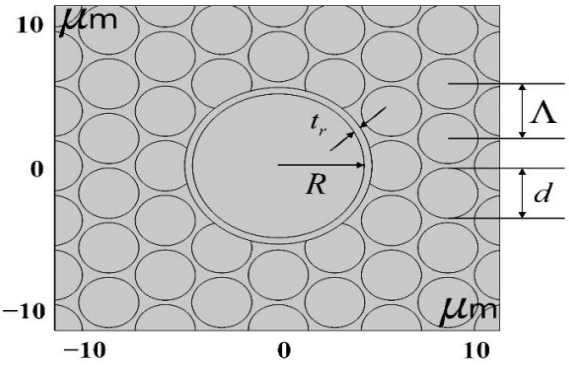

Fig.5. The schematic representation of a PCF with hollow-core and band gap cladding layer (HC-PCF) [23].

The core radius, number of cladding layers, duty cycle, background material, and core quartz-ring thickness are the main factors that affect HC-PCF performance. Core confinement loss, optical power, and effective mode area are influenced by the core diameter and related thickness of the core quartz-ring. The optical power of the core is enhanced and the confinement loss is lowered when the core quartz-ring relative thickness is varied to be of 2.0 times the spacing of neighboring air holes. The best results for confinement loss and core optical power are obtained at a core quartz-ring relative thickness of 2.0, a core radius of 1.8 times the distance between neighboring air holes, and eight cladding layers. This structure has an extremely high optical power and the confinement loss is extremely low [23].

The bandwidth of the confinement loss for enhanced configuration is 225 nm, whereas the bandwidth of transmission for the classical HC-PCF is in the nanometer range. Furthermore, in relation to the enhanced structure's transmission bandwidth, the achieved optical power is greater than 98% and the confinement loss is less

than 9.0×10^{-3} dB/m, the response variable of the effective mode field area is less than 10 μm^2, and the relative sensitivity (RS) is 95.70%. RS of the enhanced HC-PCF has increased and get close to the theoretical limit. When compared to the standard circle air hole configuration, this type of sensor configuration is appropriate for highly sensitive liquid or gas sensing.

II.3- PCF with Mono-Rectangle Core (MRC-PCF) for Blood and Skin Cancer

A strategy for accurate identification of blood and skin cancer cells using a PCF-based sensor is reported in [25]. The report proposed sensor structure that has only one rectangle forms the core area. The sensor is made up of unequal rectangular holes in the cladding area. So, the simple rectangular shape model simplifies the design and implementation process while introducing prevalent techniques [25].

ZEONEX become the fiber substance because it has some distinguishing characteristics as a fiber element. ZEONEX's main advantage is its uncharged refractive index of 1.53 in the THz frequency regime. Also, ZEONEX reclaims high chemical resistance, glass reincarnation warmth, and Moisture sensitivities [26]. Its performance is optimum at 2.0 THz and the simulation results proved its efficacy in detecting cancer cells.

The finite element method FEM is used in the model evaluation. Simulation Results show the effective material loss and confinement loss for the sensor is extremely low. Moreover, the sensitivities for detecting skin cancer cells, normal cells (basal), blood cancer cells, normal cells (Jurkat), and water are 96.61, 96.34, 96.74, 96.56, and 95.69%, respectively. Fig.6 shows the schematic illustration of the MRC-PCF model's cross section diagram.

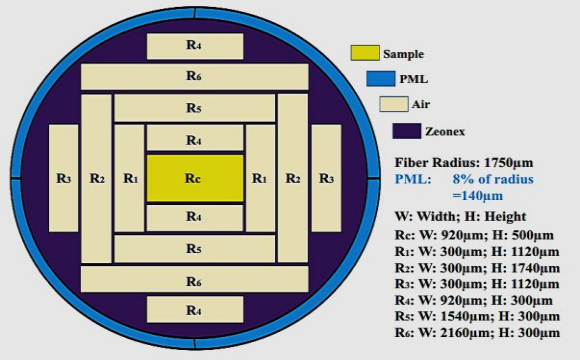

Fig. 6 The MRC model cross-sectional view [25].

This MRC-PCF has a radius of 1750 µm and PML with a thickness of 8% of its radius. The core is represented by only one rectangle signified by R_c and The core width and height are 920 µm and 500 µm, respectively. 14 rectangle air holes are arranged asymmetrically in the cladding and similar symbols are used to represent identical rectangles. For example, the core's nearest right and left rectangles are the same and thus defined as a single symbol, R_1. Using this technique results in six different rectangle patterns indicated by R_1, R_2, R_3, R_4, R_5, and R_6. Fig.6 shows the height H and width W values for each rectangle.

This PCF structure has a pitch of 310 µm and a strut distance of 10 µm between two consecutive rectangles. The hollow core PCF was chosen over porous Due to its huge layout to handle a large volume of the samples. In this model core rectangle has five various samples: normal skin cell (basal), skin cancer cell (basal), cancerous blood (Jurkat), normal blood (Jurkat), and water. The samples are infused individually into the core, and the design is being tested each time to investigate the model detection performance that specific sample is investigated.

The simulation result of the MRC-PCF structure reflects its sensitivity in detecting cancerous cells. At 2.0 THz, the proposed sensor achieves a highest relative sensitivity in sensing blood cancer cells of 96.74%. It also has a relative sensitivity of 96% for the cancer cells. At 2.0 THz, the highest value of the confinement loss measured with this sensor is 2.41×10^{-14} cm^{-1}, EML is 0.01131 cm^{-1}, the effective area A_{eff} is $2.6 \times 10^5 \mu m^2$, and Birefringence is 0.0006. Furthermore, the use of all rectangular holes in the core and cladding region facilitates design and manufacturing schemes [25].

II.4- Detecting Kerosene Adulteration in Diesel and Petrol based PCF Sensor

The quality of fuel has a massive effect on the longevity and smooth operation of any petroleum engine. Many disingenuous merchants mix kerosene, gasoline, and diesel to increase profits. This model numerical analyses a PCF based fuel adulteration sensor to resist such kerosene mixing. This sensor can detect a wide range of fuel adulteration. The typical optical parameter values, in addition to simple PCF structures based on rectangles, enhance the sensor's satisfaction and the ability of design and implementation using existing strategies [26].

Diesel and petrol are two popular bio-fuels. Because of the cost variance between kerosene, petrol, and diesel, vendors who are disingenuous will mix kerosene, diesel, and petrol to maximize revenue. In rural

areas, this mix of kerosene, diesel, and petrol is more serious. Kerosene is a difficult substance to start a fire. As a result, kerosene-mixed diesel and petrol not only impair engine performance but also cause high emissions of carbons, nitrogen monoxide, and carbon monoxide, along with other items [27-29].

There is not only one golden-standard technique for detecting fuel adulteration [30]. Nevertheless, just a few techniques are accessible, such as studying evaporations, distillations, and densities. However, none of such solutions were successful in sensing kerosene mixing with diesel and petrol. As a result, reliable accurate identification of possible contamination in fuel is a critical necessary to protect the environment and prevent illegitimate kerosene mixing.

The most recent development PCFs in chemical sensing applications has raised the standard for conventional fiber. PCFs have proven their efficiency as sensors due to a variety of advantages such as fast response, operating simplicity, high reliability, low cost, and so on. The expected sensor intends to achieve extremely high relative sensitivity in recognizing adulterated fuels while preserving low effect of CL and EML.

The PCF-based fuel adulteration sensor hollow core gives more space for the target sample to be accommodated within the core. Furthermore, because of the photonic band gap (PBG) effect and the higher core area that can support a higher amount of samples, there is a close relation between the wave and the infused sample in this PCFs [31-33]. Furthermore, when compared to porous core PCFs, the core region has more signal power, ensuring increased sensitivity [34].

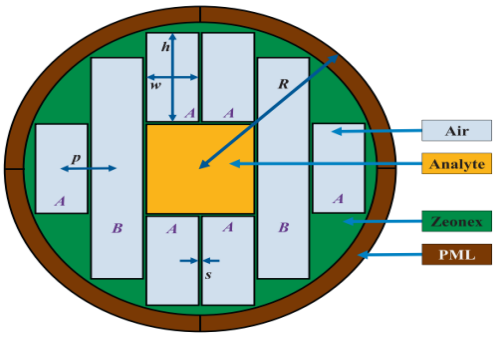

Fig.7. Model cross-sectional view for fuel contamination sensor [34].

The core is made up of a singular hollow rectangle. This proposed fuel adulteration sensor's cladding area has been created by the irregular placement of eight rectangle air holes. Based on their equal width and height, these eight rectangles can be divided into two groups: A and B. The height is h, and the width of an A-type rectangle is w, In this case h = 2w. The width of the B-type rectangles resembles that of the A-type rectangles, and the height is nearly 2.46 h. For this model, the distance among any two adjacent rectangles, known as struts, is 7.5 µm. The cladding region's pitch, p, is defined as p = (h + strut). The width and height of the mono-rectangular core is (2w + strut) and h, respectively. The proposed model has a radius R of 3.59w, which includes an internal anti - reflection coating, also known as PML at the edge, of 10% of R. PML is also immune to environmental impacts. ZEONEX has been designated as the sensor's background material [35].

This model is aimed to detect five various ratios of petrol (Pe) mixed with kerosene (Kr) (pure Pe, Pe + 20% Kr, Pe + 40% Kr, Pe + 60% Kr, Pe + 80% Kr), diesel (Di) mixed with Kr (pure Di, Di + 20% Kr, Di + 40% Kr, Di + 60% Kr, Di + 80% Kr), and pure Kr. The optical variables additionally were measured in each case. At 2.5 THz which is the optimum frequency (OF) for the optical parameters for pure petrol (Pe) CL is 9.50 x 10^{-15} cm^{-1}, effective area A_{eff} is 334,610 $(\mu m)^2$, EML is 0.0077928 cm^{-1}, Sensitivity in x- direction is 98.67 %, and Sensitivity in y- direction is 98.68 %. For Pure Kerosene (Kr): CL is 1.68 x 10^{-14} cm^{-1}, effective area A_{eff} is 332,350 $(\mu m)^2$, EML is 0.00790 cm^{-1}, and Sensitivity in y-direction is 98.83 %. Also for Pure Diesel (Di): CL is 1.58 x 10^{-14} cm^{-1}, effective area A_{eff} is 331,220 $(\mu m)^2$, EML is 0.00796 cm^{-1}, Sensitivity in x- direction is 98.89 %, and Sensitivity in y- direction is 98.90 % [34].

To evaluate different optical properties, this chemical sensor based on PCF was analyzed numerically. This numerical investigation and sensor simulation in the THz regime is carried out using FEM. Based on simulation results, this sensor has a CL of 10^{-15} cm^{-1}, and an EML of less than 0.008 cm^{-1}. Furthermore, this model has an extremely high relative sensitivity of 98.68% for sensing adulterated fuels. Nevertheless, this sensor structure's simple arrangement of rectangles ensures that manufacturing is beneficial using existing processes such as the 3Dp strategy. As a result, this sensor is designed to sense fuel adulteration and thus prevent deception oil merchants' kerosene contaminated with petrol and diesel [34].

II.5- A type-b crystalline core with hexagonal cladding CC-PCF-based photonic crystal fiber

A slightly type-b crystallized core with more convenient hexagonal cladding shape CC-PCF-based photonic crystal fiber optical sensor was developed for detecting numerous blood components, including, plasma,

Red blood cells (RBCs), white blood cells (WBCs), hemoglobin, and water. This fiber has been studied in Terahertz frequency (THz) band ranging from 1.5 to 3.50 THz, with the aim of increasing relative sensitivity while minimizing confinement loss. Circle air holes were used in the symmetric arrangement of the slightly type-b crystallized core for the same analytes at the same frequency f = 1.5 THz. Furthermore, over the investigated region, dispersion (β_2), V-Parameter (V_{eff}), effective area (A_{eff}), beam divergence (θ), and spot size (W_{eff}) have been calculated [36].

When compared to the human body's total weight, Blood probably accounts for 7% of overall weight. Human blood includes over 4000 biological components, which are multi - functional body fluids [37]. Platelets, white blood cells (leukocytes), and red blood cells (erythrocytes) make up these human blood cells (thrombocytes). Plasma accounts for approximately 54.3% of total blood volume, red blood cells (RBCs) account for approximately 45%, and white cells account for approximately 0.7%. The blood's liquid component, plasma, is approximately 90% water, with the remaining 10% made up of dissolved gases, ions, proteins, nutrients, and wastes. Examination of blood samples is critical for determining the presence of numerous hematologic diseases, including Hemophilia, Myeloma, Anemia, and Thalassemia [38].

Fig.8 represents the PCF sensors cladding region, as well as a larger view of the core region. The core is made up of circular air holes of identical diameter which are arranged hexagonally. The core is made up of seven not intersecting circles. In addition, every circle has seven circle air holes, with a single air hole in the center encircled by six air holes. Initially, the shape suggests a symmetric slight type-b crystallized. The usage of the identical air hole arrangement and size throughout the core region simplifies fabrication.

Various detecting analytes such as analytes such as hemoglobin, RBCs, plasma, WBCs, and water were considered in the core region and investigated crucial sensing factors in fibers such as effective core area, CL, relative sensitivity, spot size, beam divergence, and modality. The investigated analytes refractive index is evaluated by the core region [37].

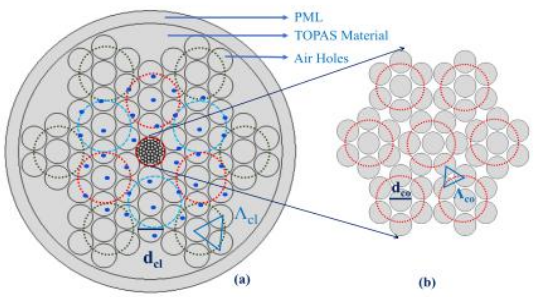

Fig.8. (a) The sensor's cladding area view. (b) Verification of the innermost core area [36].

The core has already been constructed with the core holes with d_{co} = 45.25 µm and Λ_{co} = 48.95 µm, providing design flexibility. Each circle air hole in the cladding region can construct a circle with its six neighboring air holes. The diameter of every single air hole in the cladding is the same, d_{cl} = 330.45 µm. The precise space between the centers of one air cavity and its neighboring is known as the pitch (Λ), and it determines the air filling fraction AFF. In the cladding region, AFF of 0.92 is maintained, providing fiber fabrication flexibility. A circle PML has been used here around the cladding region to absorb incoming radiation without providing reflection. TOPAS was already chosen as the proposed structure's background material. As a result of its design flexibility, the sol-gel method is preferable. The optical fiber's propagation modes are researched by employing full vector finite element method FV-FEM.

At a frequency f = 1.5 THz, this CC-PCF model has sensitivity responses of 79.39%, 80.13%, 79.91%, 80.56%, and 80.93% for water, plasma, WBCs, hemoglobin, and, RBCs respectively. The CL for WBCs, plasma, RBCs, hemoglobin, and water are 4.93×10^{-12} dB/m, 2.93×10^{-12} dB/m, 1.23×10^{-11} dB/m, 8.63×10^{-12} dB/m, and 1.13×10^{-12} dB/m, respectively. The achieved range of the effective area of the multiple blood components ranges from 1.55×10^{5} µm^2 to 1.85×10^{5} µm^2. In fiber design stage, it is also found that the core area of RBCs is 3.1416×10^{4} µm^2 and the effective area of 1.15×10^{5} µm^2 is obtained. The sensing area exceeds the designed structure by 36.6%. RBCs have a spot size of 743 µm of analyte [36].

The positive sign for this sensor is that a larger spot size, decreases beam divergence and improves beam focusing efficiency. At 1.5 THz, the RBCs, the beam divergence angle is found to be 17.89°. The higher THz spectrum, the more the beam divergence response flattens. As a result, a high level of agreement has been established for the CC-PCF sensor. The practical implementation of this model will provide superior results compared to the conventional PCF-based sensors [36].

II.6- PCF with Rectangle Porous-Core sensor

A rectangular-based, PCF with porous-core has been modelled for reliable THz wave propagation. Rectangle air holes are modelled in both the fiber cladding and core. The finite element method was employed to model this PCF-based THz waveguide in the range from 0.5 to 1.5 THz. The medium of this PCF model has been homogenized by the full vector FEM [39]. At 1.3 THz, the

model has a too-low effective material loss EML of 0.0039 cm^{-1} when versus other THz waveguides. At the same frequency, numerical analysis indicates that the model has a low dispersion of 0.3251 Ps/THz/cm. This model also has a low CL. Results are obtained at the 1.3 THz frequency because of the moderately lower EML, high power fraction, flat dispersion, and low CL. Moreover, the numerical aperture effective area, and birefringence of this model have all been measured. This PCF can be used effectively in multichannel communication as well as several domains of THz technology.

As shown in Fig.9 the total radius of the PCF is 1800 µm, which includes a PML of 140 µm. The strut is 10 µm for the core and the cladding regions. The core region is made up of 48 symmetrical small rectangles (this model is known as 48 R). Each rectangle height and width are 53.75 µm and 145 µm, respectively. The cladding layer is made up of 14 rectangles with different height and widths. R1, R2, and R3 are identical width 300 µm, and their heights are 1120 µm, 1740 µm, and 1208 µm, respectively. Once more, the widths of R4, R5, R6, and R7 are 920 µm, 1540 µm, 2160 µm, and 1608 µm, respectively, while Their heights are the same as well 300 µm.

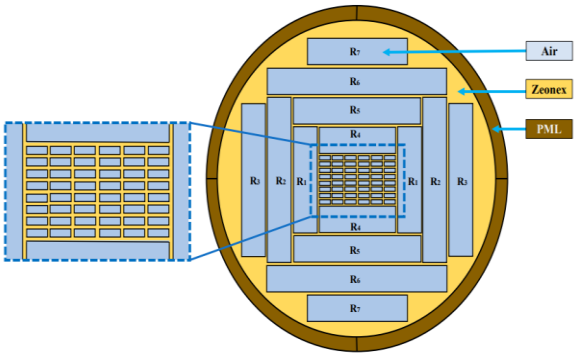

Fig.9 The PCF model cross-section [40].

ZEONEX was utilized as the PCF sensor background substance [41]. By varying strut values as well as the rectangles number in the core area, the simulation results are obtained and compared. The trial and error method is used to obtain the best PCF model.

The obtained values the dispersion is 0.3251 Ps/THz/cm, the birefringence is 0.0153, the EML is 0.0039 cm^{-1}, the CL is 1.06×10^{-12} cm^{-1}, A_{eff} is 34.00 $\times 10^4$ μm^2, the numerical aperture is 0.218, and the power fraction PF in x-polarization is 64.90%. Higher refractive index analytes achieve higher sensitivities, i.e. the air sensitivity < water sensitivity < ethanol sensitivity. The ethanol has the highest sensitivity in both Polarization Modes PMs. Sensitivity values in the x-PM for ethanol, water, and air are 74.55%, 73.20%, and 58.79%, respectively, at 1.3 THz. The sensitivity of the y-PM is 72.85%, 71.70%, and 58.73% for ethanol, water, and air, respectively. Comparing the model structure and the porosity shows the superiority and efficiency. The presented PCF might be a proper choice in the field of chemistry, telecommunication, and biomedical sensing, which is currently being investigated [40].

III. EVALUATION METRICS FOR PCF SENSORS

To determine the extent of sensor efficiency, several important parameters are measured. This section will show the equations for these parameters.

The relative sensitivity R is introduced to analyze the sensitivity of a PCF terahertz sensor. There are given by equation 1 [20]:

$$R = \frac{n_r}{n_{eff}} \times E \qquad (1)$$

Where, the refractive index of the core is n_r, effective mode index of the core is n_{eff} and the absolute sum of the light matter interface is E (the core power fraction) which can be stated as shown in equation 2 [26]:

$$E = \frac{\int_{sample} Re\,(E_x H_y, E_y H_x)\,dx\,dy}{\int_{total} Re\,(E_x H_y, E_y H_x)\,dx\,dy} \times 100\ \% \qquad (2)$$

Where, E_x and E_y are the electric domains of x, y polarization modes and H_x and H_y are stated as the magnetic domain of x, y polarization modes. E is the proportion of light power observed in the injected sample within the core to the total infused light power.

PCF-based waveguide involved two types of losses. The first is the EML which is caused primarily by the PCF configuration's background material. The usage of a porous core could provide a solution for significantly reducing EML because high porosity decreases the quantity of background material loss [43]. The EML for PCF can be calculated as shown in equation 3 [44].

$$E = \frac{\int_{mat} n_{mat}\,|E|^2 \alpha_{mat}\,dA}{2\int_{all} S_z\,dA},\ cm^{-1} \qquad (3)$$

Here, the EML is indicated by α_{eff}, the free-space permittivity denoted by ε_0, and the free-space permeability are denoted by μ_0, n_{mat} is the refractive index of the background material, E is the modal electric field, α_{mat} describes the background material absorption loss, and S_z denotes the Poynting vector z-component.

The other important loss mechanism that can limit the transmission length of the PCF waveguide is the confinement loss. The CL loss takes place because of the structure of the PCF cladding area is unsatisfactory. It is possible to reduce it by the expansion of air holes [45]. The CL loss can be expressed as shown in equation 4 [46-47]:

$$\alpha_{CL} = (\frac{A\pi F}{C}) Im(n_{eff}).\ \ cm^{-1} \quad (4)$$

Where α_{CL} is the confinement loss in cm^{-1}, f is the frequency in THz, C the velocity of light in free space in cm/s, and $Im(n_{eff})$ is the imaginary part of the refractive index of the core.

The photon energy in HC-PCFs is not totally focused on the center air hole for transmission, a percentage of optical energy is transmitted to the cladding. The effective mode field area A_{eff} is given as follows in equation 5 [25]:

$$A_{eff} = \frac{[\int\int |E(x,y)^2| \, dx \, dy]^2}{\int\int |E(x,y)^4| \, dx \, dy} \quad (5)$$

Where the electric field intensity propagation is E (x, y) for the optical fiber main mode.

The sensor's numerical aperture NA is a critical parameter to be considered. The incident light beam's angular acceptance that can be propagated across an optical fiber is identified by the NA. It is given by equation 6 [19]:

$$NA = \frac{1}{\sqrt{1+\frac{\pi A_{eff} f^2}{C^2}}} \quad (6)$$

Where the effective area indicated by A_{eff} where the optical signal propagates and the velocity of light in free space is indicated by C. As the value of the NA increases, the fiber accepts as much light as possible from the source.

One of the most severe challenges of multichannel communication is dispersion. It is required to minimize the dispersion of the PCF sensors. It occurs as a result of the effects of the background material used in fabrication. Waveguide dispersion is another type of dispersion. It is caused primarily by refraction while data is being transmitted through the core. However, some photonic crystal background materials such as ZEONEX, and TOPAS illustrates minimal dispersion changes in the Terahertz region, implying that this dispersion can be neglected. The waveguide dispersion is calculated by equation 7 [46]:

$$\beta_2 = \frac{2}{c}\frac{d\, n_{eff}}{d\, w} + \frac{w}{c}\frac{d^2 n_{eff}}{d\, w^2}.\ \ Ps/THz/\ cm \quad (7)$$

Where the dispersion is symbolized by β_2, the free-space light velocity is indicated by C, the proposed fibers effective refractive index in the core is indicated by n_{eff}, and the angular frequency is ω.

Birefringence (B) is also another different PCF optical parameter. It can be expressed by taking the distinction between the effective refractive indexes of the fiber's x and y-polarization modes. It is given by equation 8 [31]:

$$B = |n_x - n_y| \quad (8)$$

Where the refractive index of the x and y-orthogonal polarization modes is denoted by n_x and n_y respectively. Birefringence is used to measure the polarization property of PCF. The greater birefringence makes sure the effectiveness of the PCF's polarization-maintaining applications.

Details of all the used symbols and there definitions are included in appendix A at the end of the conclusion.

IV. FABRICATION FEASIBILITIES

In the THz band, the loss of the fabricated waveguide was about 0.02 cm^{-1}. There are numerous fabrication methods available for PCF models. Sol-gel casting [48], 3D-printed dies [49], extrusion [50], drawing [51], stacking, and other methods are more well-known. 3D printing [52], and Polymer-jetting rapid prototyping [53].

V. NUMERICAL MECHANISMS AND COMMERCIAL SOFTWARE PACKAGES AVAILABLE FOR THE SIMULATION OF PHOTONIC CRYSTAL FIBER SENSORS

There is no one-size-fits-all solution that helps to solve all problems without adding new difficulties. As a result, the strategy will be applied in consistent with the characteristics of the issue under consideration [55]. There are three types of computational Photonics problems: time-domain simulations, frequency domain responses, and frequency domain Eigen problems. Another Possibility of classification schemes, using mathematical methods and quantization techniques, is possible (i.e., elements or nodes). They will attempt to minimize the unknowns in order to preserve memory and time. The most well-known methods are the finite element method FEM, the finite difference time domain method FDTD,

the spectral method (SM), the plane-wave expansion method PWEM, and the boundary element method (BEM).

Full vector finite element method (FV-FEM) is a powerful tool for investigating optoelectronics. It requires less estimation time compared to other numerical approaches. The optical fiber propagating modes are investigated using FV-FEM in this work. The structures are simulated using the COMSOL Multiphysics software.

A brief description of several numerical Methods applicable to PCF chemical, biomedical, and liquid sensors is shown in Table 1, Table 2, and Table 3 respectively. According to the analytical approach used, numerous samples of COMSOL software package are listed. There are several topologies applied such as hexagonal, decagonal, mono rectangular, triangular, and rectangular structure. These PCF sensors operate at different operating frequencies with different background material for example TOPAS, ZEONEX, and SILICA GLASS, achieving effective area, birefringence, high relative sensitivity, low effective material loss, and low confinement loss.

TABLE 1
COMPARISONS OF PCF CHEMICAL SENSORS

Ref	[22] El Sevier 2021	[34] AEJ Journal 2021	[40] MDPI Sensors
Lattice type	Hexagonal	Hollow rectangle	Rectangle
Detection Target	chemical sensing	Chemical sensing	Chemical sensing
Operating frequency	1THz	2.5 THz	1.3 THz
Background Material	TOPAS	ZEONEX	ZEONEX
Effective area(μm)^2	N/A	332,350	34.0×10^4
Relative Sensitivity	82.26%	98.82%	74.55%
Birefringence	N/A	N/A	0.0153
Confinement loss	6.07×10^{-8} dB/m	1.68×10^{-14} cm^{-1}	1.06×10^{-12} cm^{-1}
EML (cm^{-1})	N/A	0.0079	0.0039
Package used	COMSOL Multiphysics	COMSOL Multiphysics	COMSOL Multiphysics
Confirmed by the author	No	Yes	Yes
Experiment /Simulation	Simulation	Simulation	Simulation

TABLE 2
COMPARISONS OF PCF BIOSENSORS

Ref	[54] 2021	[36] 2019	[55] 2021	[35] 2021	[56] 2018	[57] 2020	[40] 2020	[58] 2021
Lattice type	Circular Hollow-Core	Hexagonal	Decagonal	Mono Rectangular	Triangular lattice	Triangular lattice with ellipse	Rectangular porous core	Rectangular lattice
Detection Target	cancer	Blood Components	Blood Components	Cancer	Glucose Detection	Biosensor	Biosensor	Biosensor
Operating frequency	2.5 THz	1.5 THz	1 THz	2 THz	N/A	1 THz	1.3 THz	2.5 THz
Background Material	ZEONEX	TOPAS	TOPAS	ZEONEX	SILICA	ZEONEX	ZEONEX	ZEONEX
Effective area(m)2	2.1×10^{-8}	1.55×10^5μ	1.86×10^5 μ	2.606×10^{-7}	N/A	1.24×10^5 μ	3.4×10^5 μ	97341
Relative Sensitivity	98%	80.9%	87.68%.	96.74%	S=23.267 nm/RIU	87.02%	74.55%	95.82%
Birefringence	N/A	N/A	5.1× 10-5	0.0006	N/A	1.8× 10-2	0.0153	N/A
Confinement loss	10^{-8} dB/m	1.31×10^{-12} dB/m	1.86×10^{-9} dB/m	2.41×10^{-14} cm^{-1}	N/A	9.42×10^{-4} cm^{-1}	0.03×10^{-11} cm^{-1}	3.00×10^{-13} cm^{-1}
EML (cm^{-1})	5.5×10^{-3}	N/A	N/A	0.01131	N/A	0.009	0.0039	0.0051
Numerical Aperture	0.43	N/A	N/A	N/A	N/A	0.45	0.2179	0.2121
Package used	COMSOL Multiphysics	COMSOL Multiphysics	COMSOL Multiphysics	COMSOL Multiphysics	COMSOL Multiphysics	COMSOL Multiphysics	COMSOL Multiphysics	COMSOL Multiphysics
Confirmed by the author	Yes	Yes	No	Yes	No	No	Yes	Yes
Experiment /Simulation	Simulation	Simulation	Simulation	Simulation	Simulation	Simulation	Simulation	Simulation

TABLE 3
COMPARISONS OF PCF LIQUID SENSORS

Ref	[23] sensors 2021	[40] MDPI Sensors	[59] Photonics
Lattice type	Hollow- Core (Quartz-Ring)	Rectangle	Hexagonal
Detection Target	Liquid sensing	Liquid sensing	Liquid sensing
Operating frequency	λ=1.55 µm	1.3 THz	λ = 1.3 µm
Background Material	SILICA GLASS	ZEONEX	SILICA
Effective area(µm)^2	123.05	34.0×10^4	1.521
Relative Sensitivity	99.85%	74.55%	74.50%
Birefringence	N/A	0.0153	0.000386
Confinement loss	7.31×10^{-5} dB/m	1.06×10^{-12} cm^{-1}	6.76×10^{-11} dB/m
EML (cm-1)	N/A	0.0039	N/A
Package used	COMSOL Multiphysics	COMSOL Multiphysics	COMSOL Multiphysics
Confirmed by the author	Yes	Yes	No
Experiment /Simulation	Simulation	Simulation	Simulation

VI. CHALLENGES AND SOME NOVEL TRENDS OF PHOTONIC CRYSTAL FIBER

The comparative study demonstrates that the PCF sensing technology is rapidly expanding. An overall assessment of PCF sensing and the possible options provided by these fibers are studied. This study demonstrates their significant contribution to optical sensing technology. In this part we introduce the main challenges in addition to some novel trends which mentioned below:

A. Topology Challenges for Photonic Crystal Fiber Sensors

It is critical to identify the best photonic crystal fiber architecture configuration as a sensor. This topic of research has been investigated many years ago and is still ongoing because there are many types of topologies that have not yet been designed. It is extremely difficult to have a topology that covers all the required merits. The best application is determined by the requirements, results in obtaining the optimal values of design parameters for optimization.

It has been revealed that PCF structure provides the best research prospects for designing sensors that may be used in a variety of applications. However, it demands studying a huge search area with suitable topological structure factors to identify the construction of the PCF design that generates the necessary visual response for an effective implementation. Evaluation measures are one of the most difficult topics. The Trial and error-based techniques have yielded significant results for PCFs design. On the other hand, these procedures are time-consuming and the design may be ineffective as well.

Several of the optimum structures are challenging to produce, if not impossible. The final design of the density-based topology optimization algorithms may have a lot of intermediate aspects, which makes it challenging to precisely identify structural boundary. On the other side, research into optimum design experiments for PCFs is not very widespread. This area deserves more study and cross-disciplinary collaboration. For designing structural materials, both gradient topology optimization GTO and Non-gradient topology optimization NGTO strategies are frequently utilized. Sensitivity analysis is not required when using NGTO, and it is simple to implement for any new issues. The computational effectiveness of NGTO strategies for topology optimization needs to be increased in comparison to GTO methods. Due to the fact that topology optimization issues are both extremely nonlinear and non-convex, as shown by Sigmund [60], neither GTO nor NGTO can ensure a global optimum [61].

B. Novel Trends

In this respect, Deep Neural Networks DNN opens the way up for rapid prediction. Establishing a huge amount of data one among the most popular difficult difficulties when constructing a neural network. To compensate for the same issue, auto-encoder (AE) networks are used to achieve data augmentation. AE and DNN can be used for predicting technological platforms for a PCF-based temperature sensor [62-63]. A solid-core PCF's effective index, confinement loss, effective mode area, and dispersion can all be evaluated using machine learning algorithms. These artificial neural network-based machine learning techniques can predict the aforementioned optical qualities with high accuracy. The Feed-forward artificial neural networks can forecast the output undetermined design parameters more rapidly than traditional numerical simulation methods using simple and quick training methods [64].

VII. CONCLUSIONS

PCF sensors presented in this literature review are used for different sensing applications. Multiple configurations and their effects on reshaping the PCFs application are reviewed. The behavior of the PCF sensors

depends upon many different parameters such as the sensor design, background material, operational wavelength, and the analyte refractive index to be detected. The same PCF topology can be used for different sensing purposes. COMSOL Multiphysics simulation is the most common software tool for simulating such sensors based on calculations.

Appendix A.

See table 4

TABLE 4 DESCRIPTION OF USED SYMBOLS

Symbol Unit	Symbol Description	Unit
Λ	pitch	µm
d	diameter	µm
CL	confinement losses	dB/m or cm^{-1}
A_{eff}	mode field areas	μm^2
n_{PML}	Refractive index of PML	unitless
n_{eff}	Effective refractive index of the core	unitless
f	optical powers	%
PF	Power fraction	%
EML	Effective material loss	cm^{-1}
R	the radius	µm
t_r	core quartz-ring thickness	µm
W	Width	µm
H	Height	µm
R	Sensitivity	%
f	Frequency	THz
β_2	Dispersion	Ps/THz/cm
AFF	air filling fraction	unitless
NA	numerical aperture	unitless
π	22/7	unitless
C	the velocity of light in free space	Cm/s

References

[1] E. Yablonovitch, "Inhibited spontaneous emission in solid-state electronics", Phys. Rev. Lett. 1987, 58, 2059–2062.

[2] A. Blanco, E. Chomski, S. Grabtchak, M. Ibisate, S. John, et al. "Large-Scale synthesis of a silicon photonic crystal with a complete three-dimensional band gap near 1.5 micrometers", Nature, 405, 437–440, 2000.

[3] J.C. Knight, T.A. Birks, P.J. Russell, D.M. Atkin, "All-Silica single-mode optical fiber with photonic crystal cladding: Errata", Opt. Lett., 22, 484–485, 1997.

[4] R.K. Chourasia, V. Singh, "Estimation of photonic band gap in the hollow core cylindrical multilayer structure", Superlattices Microstruct, 116, 191–199, 2018.

[5] V. Kaur and S. Singh,'' Extremely sensitive multiple sensing ring PCF sensor for lower indexed chemical detection,'' Sens. Bio-Sens. Res., vol. 15, pp. 12–16, Sep. 2017.

[6] V. Kaur, S. Singh, "A dual-channel surface Plasmon resonance biosensor based on a photonic crystal Fiber for multianalyte sensing", J. Comput. Electron. 18 (1), 319–328, 2019.

[7] B.K. Paul, M.A. Haque, K. Ahmed, S. Sen, "A Novel Hexahedron Photonic Crystal Fiber in Terahertz Propagation: Design and Analysis", Photonics 6 (1), 2019.

[8] J. Sultana, M.R. Islam, M. Faisal, K.M.A. Talha, M.S. Islam, "Design and analysis of a ZEONEX based diamond-shaped core kagome lattice photonic crystal fiber for T-ray wave transmission", Opt. Fiber Technol. 47, 55–60,2019.

[9] T. Reena, S. Saini, A. Kumar, Y. Kalra, R.K. Sinha, "Rectangular-core large-mode-area photonic crystal fiber for high power applications: Design and analysis", Appl. Opt. 55 (15), 4095, 2016.

[10] M. Morshed, M. Imran Hassan, T.K. Roy, M.S. Uddin, S.M. Abdur Razzak, "Microstructure core photonic crystal fiber for gas sensing applications", Appl. Opt. 54 (29) ,8637, 2015.

[11] M.B. Hossain, E. Podder, "Design and investigation of PCF-based blood components sensor in terahertz regime", Appl. Phys. A Mater. Sci. Process. 125 (12), 861, 2019.

[12] V. Kaur, S. Singh, "Design approach of solid-core photonic crystal fiber sensor with sensing ring for blood component detection", J. Nanophoton. 13 (2) 026011, May 2019.

[13] P. Sharma, P. Sharan, "Design of photonic crystal-based biosensor for detection of glucose concentration in urine", IEEE Sensors J. 15 (2), 1035–1042, 2015.

[14] A.A. Rifat, et al., "Surface Plasmon resonance photonic crystal fiber biosensor: a practical sensing approach", IEEE Photon. Technol. Lett. 27 (15), 1628–1631, 2015.

[15] Y. Guo, J. Li, S. Li, L. Jin Sun, Y. Liu, et al., "Amphibious sensor of temperature and refractive index based on D-shaped photonic crystal fiber filled with liquid crystal", Liq. Cryst. 47 (6), 882–894, 2019.

[16] K. Ahmed, F. Ahmed, S. Roy, B.K. Paul, M.N. Aktar, D. Vigneswaran, M.S. Islam, "Refractive Index Based Blood Components Sensing in Terahertz Spectrum", IEEE Sens. J. 19 (9), 2019.

[17] I.K. Yakasai, P.E. Abas, H. Suhaimi, F. Begum, Low loss and highly birefringent photonic crystal fiber for terahertz applications, Optik 206,1643221, 2020.

[18] S.F. Kaijage, Z. Ouyang, X. Jin, "Porous-core photonic crystal fiber for low loss terahertz wave guiding", IEEE Photonics Technol. Lett., 25, 1454–1457, 2013.

[19] M. Skorobogatiy, A. Dupuis, "Ferroelectric all-polymer hollow Bragg fibers for terahertz guidance", Appl. Phys. Lett., 90, 113514, 2007.

[20] H. Ademgil, "Highly sensitive octagonal photonic crystal fiber-based sensor", Opt. Int. J. Light Electron Opt. 125 (20), 6274–6278, 2014.

[21] S. Asaduzzaman, K. Ahmed, T. Bhuiyan, T. Farah, Hybrid photonic crystal fiber in chemical sensing, Springer plus 5 (1), June 2016.

[22] S.Abdullah, M.Al-Shafi, and K.Ashad, "Hexagonal photonic crystal Fiber (H-PCF) based optical sensor with high relative sensitivity and low confinement loss for terahertz (THz) regime", Sensing and Bio-Sensing Research | Journal | ScienceDirect.com by Elsevier, Vol.(30), 100377,December 2020.

[23] B. Wan, L. Zhu, X. Ma, T. Li, J. Zhang, "Characteristic Analysis and Structural Design of Hollow-Core Photonic Crystal Fibers with Band Gap Cladding Structures", Sensors 2021, 21, 284.

[24] Available online: https://www.thorlabs.us /thorproduct.cfm? Part number =HC19-1550 (Accessed on 20 December 2020).

[25] M. A. Eid., A. Rashed, A. Al-Mamun, E. Podder, "Mono-Rectangular Core Photonic Crystal Fiber (MRC-PCF) for Skin and Blood Cancer Detection,"Plasmonics, 16:717–727, 2021.

[26] M.B. Hossaina, E. Podder, A.A.M. Bulbul, H.S. Mondal, "Bane chemicals detection through photonic crystal fiber in THz regime", Opt. Fiber Technol. 54, 102102, Jan. 2020.

[27] K. Boadu, "Effects of Adulteration on Diesel Oil with Kerosene Fuel in Ghana", Journal of Applied Sciences and Environmental Management 23 (7), 1195–1200, 2019.

[28] B.P. Vempatapu, D. Tripathi, J. Kumar, P.K. Kanaujia, "Determination of kerosene as an adulterant in diesel through chromatography and high-resolution mass spectrometry", SN, Applied Sciences 1, (6) 614, 2019.

[29] Y.S. Jin, G.J. Kim, C.-H. Shon, S.G. Jeon, J.I. Kim, "Analysis of Petroleum Products and Their Mixtures by Using Terahertz Time Domain Spectroscopy", J Korean Chem Soc 53, 879– 1885, 2008.

[30] A.K. Gupta, R. Sharma, "A new method for estimation of automobile fuel adulteration", Air Pollution, 357–370, 2010.

[31] M. Ebnali-Heidari, F. Koohi-Kamali, A. Ebnali-Heidari, M.K. Moravvej-Farshi, B.T. Kuhlmey, "Designing Tunable Microstructure Spectroscopic Gas Sensor Using Optofluidic Hollow-Core Photonic Crystal Fiber", IEEE J. Quantum Electron. 50 (12), 1–8, 2014.

[32] X. Yang, C. Shi, D. Wheeler, R. Newhouse, B. Chen, J.Z. Zhang, C. Gu, "High-sensitivity molecular sensing using hollow-core photonic crystal fiber and surface-enhanced Raman scattering", J. Opt. Soc. Am. A 27 (5), 977–984, 2010.

[33] S. Liu, W. Gao, H. Li, Y. Dong, H. Zhang, "Liquid-filled simplified hollow-core photonic crystal fiber", Opt. Laser Technol. 64, 140–144, 2014.

[34] A.A.-M Bulbul, A.N.Z. Rashed, H.M. El-Hageen, A.M. Alatwi, "Design and numerical analysis of an extremely sensitive PCF-based sensor for detecting kerosene adulteration in petrol and diesel", Alexandria Engineering Journal, 60 (6), pp. 5419-5430, 2021.

[35] M.S. Islam, J. Sultana, J. Atai, D. Abbott, S. Rana, M.R. Islam, "Ultra low-loss hybrid core porous fiber for broadband applications", Appl. Opt. 56 (4), 1232–1237, 2017.

[36] K. Ahmed, F. Ahmed, S. Roy, B. K. Paul, M. N. Aktar, D. Vigneswaran, and M. S. Islam, "Refractive Index-Based Blood Components Sensing in Terahertz Spectrum," IEEE Sensors J., vol. 19, no. 9, pp. 3368-3375, May 2019.

[37] P. Sharma and P. Sharan, "Design of photonic crystal based ring resonator for detection of different blood constituents," Opt. Commun., vol. 348, pp. 19–23, Aug. 2015.

[38] S. Singh and V. Kaur, "Photonic crystal fiber sensor based on sensing ring for different blood components: Design and analysis," in Proc. 9th Int. Conf. Ubiquitous Future Netw. (ICUFN), pp. 399–403, Jul. 2017.

[39] J. Stolz, P. Fideu, A."Herrmann, Homogenization of Fiber Composite Material Properties: An Adaptive Mulitiphysics Implementation", Available online: https://www.comsol.it/paper /download/570781/stolz_ paper. Pdf, Oct. 2020.

[40] A. A. Bulbul, F. Imam, M. A. Awal, and M. A. Parvez, "A Novel Ultra-Low Loss Rectangle-Based Porous-Core PCF for Efficient THz Waveguidance: Design and Numerical Analysis", Sensors, 20, 6500, http://www.mdpi.com/journal/sensors, 2020.

[41] G. Woyessa, A. Fasano, C. Markos, A. Stefani, H.K. Rasmussen, O. Bang, "ZEONEX microstructured polymer optical fiber: Fabrication friendly fibers for high temperature and humidity insensitive Bragg grating sensing", Opt. Mater. Express, 7, 286–295, 2017.

[42] X. Meng, J. Li, Y. Guo, S. Li, Y. Wang, W. Bi, H. Lu, "An optical-fiber sensor with double loss peaks based on surface Plasmon resonance", Optik 216 ,164938, Aug. 2020.

[43] M.S. Islam, J. Sultana, A.A. Rifat, A. Dinovitser, B.W.-H. Ng, D. Abbott, "Terahertz sensing in a hollow core photonic crystal fiber", IEEE Sens. J., 18, 4073–4080, 2018.

[44] G. Hasanuzzaman, S. Rana, M.S. Habib, "A novel low loss, highly birefringent photonic crystal fiber in THz regime. IEEE Photonics Technol", Lett., 28, 899–902, 2016.

[45] M.S. Islam, S. Rana, M.R. Islam, M. Faisal, H. Rahman, J. Sultana, "Porous core photonic crystal fiber for ultra-low material loss in THz regime", IET Commun., 10, 2179–2183, 2016.

[46] J. Sultana, M.S. Islam, M. Islam, D. Abbott, "High numerical aperture, highly birefringent novel photonic crystal fiber for medical imaging applications", Electron. Lett., 54, 61–62, 2017.

[47] A.A.M. Bulbul, R.H. Jibona, S.K.D. Das, T. Roy, , M.A. Saha, M.B. Hossain, "PCF Based Formalin Detection by Exploring the Optical Properties in THz Regime", Nanosci. Nanotechnol. Asia, 10, 1–8, 2020.

[48] R.T. Bise, D.J. Trevor, "Sol-gel derived microstructure fiber: Fabrication and characterization", In Optical Fiber Communication Conference, Optical Society of America: Anaheim, CA, USA, p. OWL6, 2005.

[49] H. Ebendorff-Heidepriem, J. Schuppich, A. Dowler, L. Lima-Marques, T.M. Monro, "3D-printed extrusion dies: A versatile approach to optical material processing", Opt. Mater. Express, 4, 1494–1504, 2014.

[50] A. Ghazanfari, Li. W. M.C. Leu, G.E. Hilmas, "A novel freeform extrusion fabrication process for producing solid ceramic components with uniform layered radiation drying", Addit. Manuf., 15, 102–112, 2017.

[51] G. Barton, M.A. van Eijkelenborg, G. Henry, M.C. Large, J. Zagari, "Fabrication of microstructured polymer optical fibers", Opt. Fiber Technol, 10, 325–335, 2004.

[52] J. Yang, J. Zhao, C. Gong, H. Tian, L. Sun, P. Chen, L. Lin, W. Liu, "3D printed low-loss THz waveguide based on Kagome photonic crystal structure", Opt. Express, 24, 22454–22460, 2016.

[53] Z. Wu, W.-R. Ng, M.E. Gehm, H. Xin, "Terahertz electromagnetic crystal waveguide fabricated by polymer jetting rapid prototyping", Opt. Express, 19, 3962–3972, 2011.

[54] A. Habib, A. N. Z. Rashed, H. M. El-Hageen, and A. M. Alatwi, ''Extremely sensitive photonic crystal fiber–based cancer cell detector in the terahertz regime,'' Plasmonics, vol. 16, no. 4, pp. 1297–1306, Aug. 2021.

[55] A. Kumar, P. Verma, and P. Jindal, ''Decagonal solid core PCF based refractive index sensor for blood cells detection in terahertz regime,'' Opt. Quantum Electron., vol. 53, no. 4, pp. 1–13, Apr. 2021.

[56] A. Natesan, K. P. Govindasamy, T. R. Gopal, V. Dhasarathan, and A. H. Aly, ''Tricore photonic crystal fibre based refractive index sensor for glucose detection,'' IET Optoelectron., vol. 13, no. 3, pp. 118–123, Jun. 2019.

[57] N. A. N. B. Suhaimi, I. K. Yakasai, E. Abas, S. Kaijage, and F. Begum, ''Modelling and simulation of novel liquid-infiltrated PCF biosensor in terahertz frequencies,'' IET Optoelectron., vol. 14, no. 6, pp. 411–416, Dec. 2020.

[58] A. A. M. Bulbul, A. Z. Kouzani, M. P. Mahmud, and A. A Nahid, "Design and numerical analysis of a novel rectangular PCF (R-PCF)-based biochemical sensor (BCS) in the THz regime," International Journal of Optics, 1-16, 2021.

[59] A. M. Maidi, I. Yakasai, P. E. Abas, M. M. Nauman, R. A. Apong, S. Kaijage, and F. Begum, "Design and Simulation of Photonic Crystal Fiber for Liquid Sensing", Photonics, 8, 16, 2021.

[60] Sigmund, Ole. "On the usefulness of non-gradient approaches in topology optimization." Structural and Multidisciplinary Optimization 43 (2011): 589-596 .

[61] W. Li, F. Meng, Y. Chen, Y. F. Li, and X. Huang, ''Topology optimization of photonic and phononic crystals and metamaterials: A review,'' Adv. Theory Simulations, vol. 2, no. 7, pp. 1–22, 2019.

[62] S. Sridevi, T. Kanimozhi, N. Ayyanar, S. Chugh, M. Valliammai and J. Mohanraj, "Deep Learning Based Data Augmentation and Behavior Prediction of Photonic Crystal Fiber Temperature Sensor," *IEEE Sensors Journal*, vol. 22, no. 7, pp. 6832-6839, 2022.

[63] N. M. Azzam., O. E. Khedr, S. El-Rabaie and A. S. Al Khalaf. "Literature Review: On-chip Photonic Crystals and

Photonic Crystal Fiber for Biosensing and Some Novel Trends." IEEE Access PP. 2022.

[64] S. Chugh, A. A. Gulistan, S. Ghosh, and B. M. A. Rahman," Machine learning approach for computing optical properties of a photonic crystal fiber", Optics Express, V. 27, No. 25, 2019.